RSC Advances

PAPER

View Article Online
View Journal | View Issue

Cite this: *RSC Adv.*, 2026, **16**, 17176

Effect of water molecules on the diffusions of alkali metal ions in two-dimensional transition metal sulfides

Jing Tian and Xiao Gu *

Two-dimensional sulfide materials are promising cathode materials for alkali-ion batteries. However, the presence of water can significantly impact their performance. Using density functional theory, this study reveals how water molecules influence alkali metal ion diffusions in MS_2 (M = Mo, V, Ni) cathodes. In a pristine MS_2 layer, the diffusion barrier for a single ion along the sulfur path is high. When water is introduced into the interlayer, it forms hydrated alkali metal ions. We found that among the three two-dimensional transition metal sulphides (MoS_2, WS_2, NiS_2), Li exhibits the highest capacity for accommodating hydrated ions. The diffusion of these hydrated ions results in a significantly lower energy barrier. This reduction in the diffusion barrier becomes more substantial as the number of water molecules increases. These findings indicate that strategically increasing interlayer water concentration could be essential for enhancing the performance of two-dimensional sulfide-based batteries.

Received 31st January 2026
Accepted 25th March 2026

DOI: 10.1039/d6ra00840b

rsc.li/rsc-advances

1 Introduction

In recent years, atmospheric greenhouse gases (GHGs, mainly including CO_2, CH_4, and N_2O) have shown a significant growth trend, in which fossil fuel combustion and agricultural activities are the main sources of GHG emissions, and these anthropogenic GHG emissions have become the main cause of the current global climate change, and also constantly threaten the life and survival of human beings.[1] Therefore, the development and application of renewable energy is a key solution to the problems of fossil energy depletion and climate change. In recent years, the proportion of renewable energy in the global energy structure has increased significantly; on the one hand, the progress of energy storage technology and the decline of energy costs have promoted the large-scale application of clean energy such as solar energy and wind energy; on the other hand, the rapid development of smart grids effectively alleviates the intermittency of renewable energy power generation. At the same time, the improvement of national policy support mechanisms and international co-operation continues to promote the transformation process of the energy system, and renewable energy has gradually become the core pillar of the energy system.[2]

Among them, lithium-ion batteries (LIBs) have become the core technology in modern energy storage due to their high energy density, excellent power characteristics, and outstanding cycling stability. Research over the past decades has shown that LIBs have a highly reversible lithium-ion embedding/de-embedding mechanism and stable electrode/electrolyte interface characteristics, which have enabled LIBs to demonstrate irreplaceable application advantages in portable electronic devices, electric vehicles, and large-scale energy storage, leading the development of electrochemical energy storage technology.[3] Although lithium-ion batteries have been commercially applied in portable electronic devices and have shown excellent application prospects in electric vehicle power batteries and smart grid energy storage. With the rapid development of the electric vehicle industry, the upper limit of the theoretical energy density of the existing commercialized lithium-ion battery system (about 300–350 W h kg^{-1}) is difficult to meet the rapidly growing energy storage market demand.[4,5] Therefore, the development of new battery systems based on crustal abundance elements is imminent. Sodium, as a neighbouring homologue of lithium, has similar alkali metal electrochemical properties and is abundant and widely distributed, making it an alternative energy storage material with great development potential.[6–8] Similarly, potassium-ion batteries (KIBs) have a significant resource advantage due to their high crustal abundance of potassium, and KIBs are able to exhibit higher conductivity than LIBs and SIBs batteries.[9]

As we all know, batteries are mainly composed of two parts: electrolyte and electrode materials. Conventional electrolytes can be classified as organic liquid electrolytes, polymer electrolytes, inorganic solid electrolytes, ionic liquid electrolytes, and aqueous electrolytes.[10] Among them, organic solvents are the most widely used electrolytes, but because organic electrolytes are flammable and explosive, they can easily react with electrodes to cause thermal runaway, and polymer electrolytes, with their low thermal stability and low ignition point, can also

School of Physical Science and Technology, Ningbo University, Ningbo 315211, China. E-mail: guxiao@nbu.edu.cn

cause explosions and fire accidents when used improperly.[11,12] Solid electrolytes are relatively safer, but have very low conductivity and slow ion transport kinetics, which can affect battery performance.[13] Whereas ionic liquid electrolytes are more costly, and their high viscosity can also lead to lower conductivity.[14] Comparatively speaking, aqueous electrolytes are inherently non-flammable and have a higher ionic conductivity at a lower cost, making them a very good choice for us.[15–17] In addition to the electrolyte, the structure and properties of the electrode material determine the energy density, voltage, capacity, and cycle life of the battery.[18] Battery materials can be classified into 1D, 2D, and 3D materials based on their dimensionality[19] Among other things, one-dimensional materials can significantly accelerate unwanted side reactions with electrolyte solutions.[20] Three-dimensional materials suffer from volume expansion, low multiplier capacity, and poor cycling stability during charge/discharge processes.[21] Whereas the large specific surface area of 2D materials increases the contact area with the electrolyte, which can improve ion transport kinetics.[22] This superionic conduction property reduces the ion migration barrier for ultrafast ion transport.[23] The main types of 2D electrode materials are graphene and graphene analogues, sulphur generators, metal oxides/hydrides, MXene, and mono-elements, among which transition metal oxides (TMOs), transition metal hydroxides (TMHs), transition metal disulphides (TMDs), and MXenes, which have been widely investigated as materials for potential applications in LIB electrodes.[24] Among the sulphur compounds they usually have an open structure with weak interlayer van der Waals forces, which may facilitate rapid intercalation/decalcification of ions (Li, Na).[25] Higher reversible capacity can be achieved compared to other electrode active materials.[26]

Two-dimensional sulphur compounds can be prepared by a variety of synthetic methods, such as chemical vapour deposition (CVD),[27] hydrothermal methods,[28] sol–gel methods,[29] *etc.*, which are highly controllable and universally applicable. There are three main phases, 1T, 2H, and 3R, of two-dimensional sulphur compounds represented by MoS_2.[30] Among them, the charge transfer performance of MoS_2 in the 2H phase is poor, which will lead to faster cell capacity decay and poor multiplication performance.[30,31] Whereas 3R-phase materials may have a high defect density and thus poor stability.[32] In comparison, 1T-phase MoS_2 has more stable electrochemical properties, and the metallic conductivity and excellent hydrophilicity of 1T-MoS_2 can facilitate effective charge transfer and allow the aqueous electrolyte to be sufficient to access the 2D interlayer channels of 1T-MoS_2.[33] It was also observed that the anode specific capacity in sodium-ion batteries was 224 mA h g^{-1} at a high current density of 8 A g^{-1} when 1T-phase MoS_2 was used as the electrode material, and this excellent performance was also attributed to its enhanced kinetics and stable 1T octahedral coordination.[34]

Using first-principles calculations, we reveal that water molecules promote the diffusion of Li, Na, and K ions in two-dimensional sulfide battery materials. Diffusion barrier calculations for systems with 1–3 water molecules confirm this enhancing effect.

2 Computational details

In this study, all calculations were based on density functional theory (DFT) and simulated using the Vienna *Ab initio* Simulation Package (VASP).[35,36] The generalized gradient approximation (GGA) of the Perdew–Burke–Ernzerhof (PBE)[37] exchange–correlation function is used in the calculations and combined with the projector augmented-wave (PAW)[38] method to describe the interactions between the nucleus and valence electrons. In the plane-wave basis set, the kinetic cutoff energy of the wave function was set to 450 eV, and the convergence criterion for the electron energies was 10^{-6} eV. The forces converge to 0.05 eV $Å^{-1}$ for all unconstrained atoms and by employing Grimme's density functional theory-density functional density correction (DFT-D2)[39,40] scheme, the long-range van der Waals (vdW) interactions governing the stability of the dominant layered MS_2 structure were precisely characterized. The irreducible portion of the Brillouin zone was sampled using a $1 \times 1 \times 1$ Monkhorst–Pack *k*-point grid. To calculate the diffusion energy barrier, the climbing image nudged elastic band (CI-NEB) method was used to determine the transition states, and longer diffusion paths were segmented to simulate the atomic migration process.

3 Results and discussion

Two-dimensional metal disulfides exhibit a unique layered crystal structure, as shown in Fig. 1(a). The structure consists of layers of metal atoms sandwiched between two layers of sulfur (S) atoms, forming a hexagonal lattice. In this article, we discuss three different 2D transition metal sulfides, namely MoS_2, VS_2, NiS_2, which have similar layered structures. For example, MoS_2 is a typical 2D transition metal disulfide with a unique layered crystal structure, its basic structure consists of a molybdenum (Mo) atomic layer sandwiched between the upper and lower sulfur (S) atomic layers, forming an 'S–Mo–S' layer structure. This structure belongs to the hexagonal crystal system, with the Mo atom in the center of the hexagon and the surrounding S atoms forming a flat triangular prism. The Mo–S bond length is about 2.42 Å, the V–S bond length is about 2.36 Å, and the Ni–S bond length is about 2.37 Å. They bond within the layer by strong covalent bonds, while the layers interact with each other by weak van der Waals forces.

As shown in Fig. 1(b), there are four possible occupation sites in 2D transition metal sulfides: Top-M, Top-S, Bridge, and Hollow sites. The activity of these sites not only affects the electronic properties and catalytic performance of the material, but also determines the path and efficiency of ion migration. Therefore, the optimal occupation sites for ions should be determined before migration. The binding energy of alkali metal ions MS_2 was calculated using the following formula: $E_b = E[MS_2] + E[Y] - E[YMS_2]$; the greater the binding energy, the more stable the system will be. In Table 1, the binding energies of the three materials at different adsorption sites are given, and we find that for different materials, alkali metal ions are adsorbed above M or at the bridge point with the highest binding energy. In the calculation process, the alkali metal ions are more inclined to be above M (Top-M), which may be because

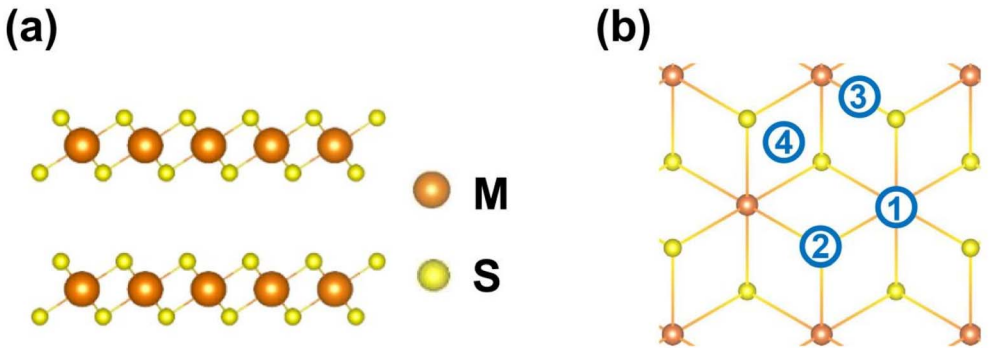

Fig. 1 (a) Side view of pristine 1T-MS_2 (M = Mo, V, Ni), where d_{Mo-Mo} (the Mo–Mo layer spacing) is 5.90 Å, d_{V-V} (the V–V layer spacing) is 5.75 Å, and d_{Ni-Ni} (the Ni–Ni layer spacing) is 6.00 Å. (b) Four available adsorption sites for metal atoms in the 1T-MS_2 monolayer. The orange and yellow spheres represent M and S atoms, the blue circles represent the four occupied sites. Respectively, labels 1 to 4 represent the Top-Mo, Top-S, Bridge, and Hollow surface sites.

Table 1 Binding energy (eV) of the four adsorption positions in 1T-MS_2 (M = Mo, V, Ni)

1T-MS_2	Ions	Top-S	Top-M	Hollow	Bridge
MoS_2	Li	3.12	3.90	3.12	3.90
	Na	2.01	2.97	2.97	2.97
	K	2.66	2.96	2.66	2.95
VS_2	Li	3.40	4.29	3.40	4.29
	Na	2.85	3.48	2.85	3.48
	K	3.00	3.38	3.38	3.38
NiS_2	Li	2.45	2.78	2.45	2.78
	Na	3.16	3.73	3.16	3.73
	K	3.23	3.61	3.23	3.61

the space above M is relatively large, and the alkali metal ions are more inclined to be in a large space. Moreover, studies have demonstrated that the intrinsic migration pathways of alkali metal ions within layered MS_2 are predominantly governed by the Top-M site transition mechanism.[41,42] Consequently, we selected the Top-M adsorption site for subsequent investigations. The results show that the transition state energy barrier that ions need to overcome in the process of migration is relatively low, the ions are not easy to be trapped to form localized traps, and the high conductivity can be maintained, and the small binding energy gap can make the ion mobility insensitive to structural deformation, which improves the cycling stability, and if the ions carry water molecules, the sites with similar binding energy can allow the hydrated ions to be dynamically adjusted without significantly increasing the total migration energy, which shows that two-dimensional sulfides are ideal for high-performance ion transport materials.

Existing research confirms that in aqueous alkali metal ion batteries, when alkali metal ions bind with four water molecules within the interlayer of two-dimensional sulphides, one water molecule dissociates from the alkali metal ions and exists in a free state.[43] Therefore, during the process of intra-layer migration, we consider the scenario where the number of coordinating water molecules is less than four for analysis. The morphology of the hydrated ions is shown in Fig. 2(a) where $Y{\cdot}2H_2O$ is linear and $Y{\cdot}3H_2O$ is planar and triangular in the optimized stable structure. Regarding the length of the Y–O bond (shown in Fig. 2(b)), the following relationship always exists as the hydration number increases: $d_{K-O} > d_{Na-O} > d_{Li-O}$. This pattern indicates that the bond length between the hydrated ions and oxygen atoms increased as the ionic radius increased. This phenomenon can be explained by the charge density of the ions and hydrogen bonding of the water molecules, where a larger ionic radius leads to a weaker electrostatic attraction between the ions and water molecules, which increases the hydration bond length. The interlayer spacing of the two-dimensional sulfide also significantly influences the stability of intercalated alkali metal ions. We calculated the binding energy of the alkali metal ions in the three materials with different layer spacings, as shown in Fig. 3. To evaluate the influence of interlayer spacing, we calculated the binding energy of Li, Na, and K ions positioned at Top-M in the two-dimensional sulfides (MoS_2, VS_2, NiS_2). Fig. 3(b) shows the binding energies of Li, Na, and K when the layer spacing of MoS_2 is from 6.0 Å to 9.0 Å, where the binding energy of Li, Na, and K reaches the maximum when the layer spacing is 6.5 Å, 7.5 Å, and 8.5 Å, respectively. Similarly, for VS_2 and NiS_2 in Fig. 3(c and d), the layer spacing of Li, Na, and K to reach the maximum binding energy increases sequentially. The optimal interlayer spacing increases from Li^+ to K^+ due to their increasing ionic radii. A larger spacing is required to mitigate steric repulsion with the sulfur layers. Consequently, determining the ion-specific optimal spacing is critical for accurate migration energy calculations.

While previous studies have established the diffusion behavior of isolated alkali metal ions in two-dimensional sulfides, the intrinsic mechanism governing ion transport in the presence of water molecules remains unexplored. In this study, we conducted a diffusion study of alkali metal ions and hydrated ions in different two-dimensional sulfides. We first analyzed the trend in the Y–O bond lengths of alkali metal ions$^+$ as the degree of hydration m increases from 1 to 3 in the 1T-MS_2 (M = Mo, V, Ni) system (as shown in Table S1). Fig. S1 demonstrates that, across different materials, as the number of coordinating water molecules increases and the hydration shell

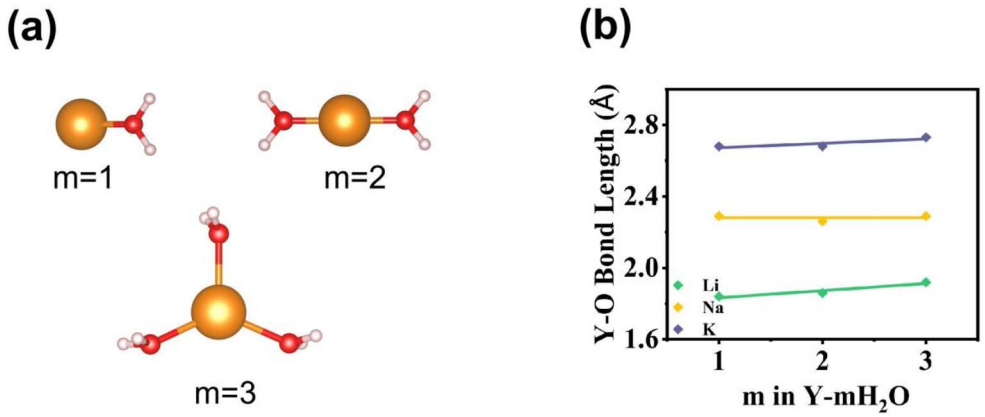

Fig. 2 (a) Gaseous hydrated ions Y·mH$_2$O (Y = Li, Na, K), where m denotes the number of water molecules bonded to Y. (b) The average bond length of Y–O ions to m in gaseous hydrated ions. The green line indicates the bond length of the Li–O (1.87 ± 0.05 Å), the orange line represents the bond length of the Na–O (2.28 ± 0.02 Å), and the purple line represents the bond length of the K–O (2.70 ± 0.03 Å).

becomes more saturated, the Y–O bond lengths for each material follow the order K > Na > Li. Fig. 4(a–c) schematics of the diffusion path for alkali metal ions (Li, Na, K) hydrated with 1–3 water molecules, and Fig. 4(d–f) the corresponding diffusion energy barriers and interlayer spacing changes as a function of hydration (0–3 H$_2$O). It can be observed that with an increase in the number of water molecules, the diffusion barrier decreases significantly. The reduction of Li is the most obvious, especially in VS$_2$ and NiS$_2$, when Li carries three water molecules, the diffusion barrier is even reduced to 0.054 eV and 0.046 eV. Na and K ions exhibit the same inverse relationship: the migration barrier decreases with increasing hydration. The observed minimum in the diffusion barrier at a hydration level of three water molecules indicates that water content is a critical factor in promoting alkali metal ion diffusion within the sulfide structure. This is partially due to that the addition of water

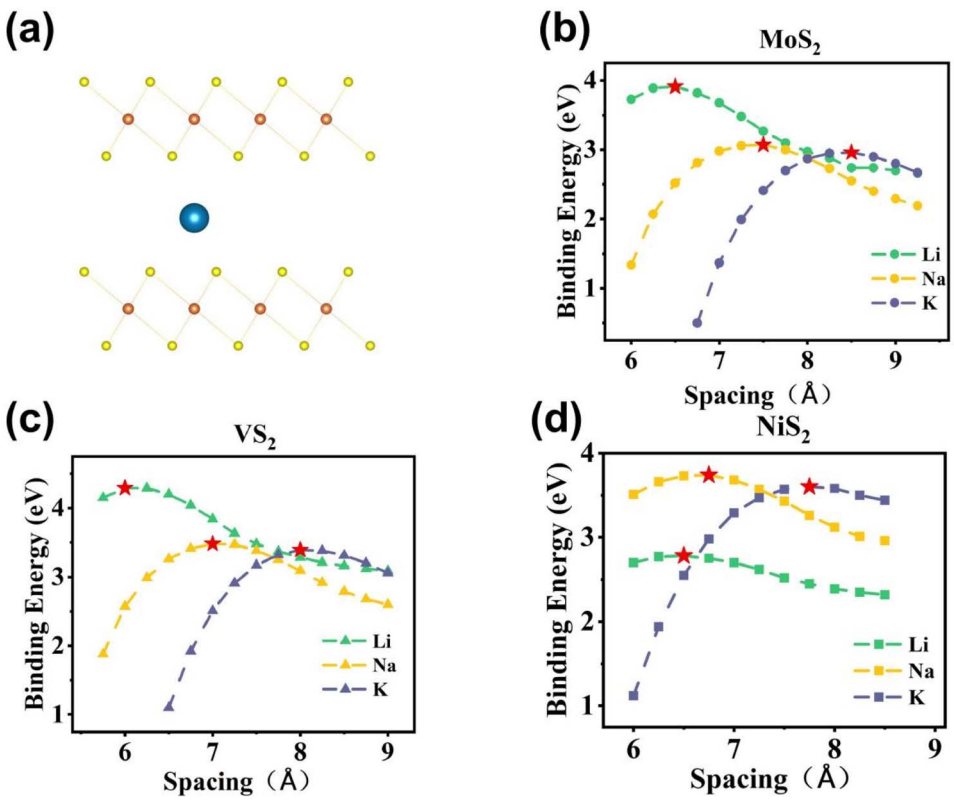

Fig. 3 Effect of layer spacing of two-dimensional sulfides on the binding energy of alkali metal ions. (a) The Top-M position of alkali metal ions in the MS$_2$ layer. (b–d) The relationship between the binding energy and the layer spacing when the alkali metal ions are intercalated in the MoS$_2$, VS$_2$, and NiS$_2$.

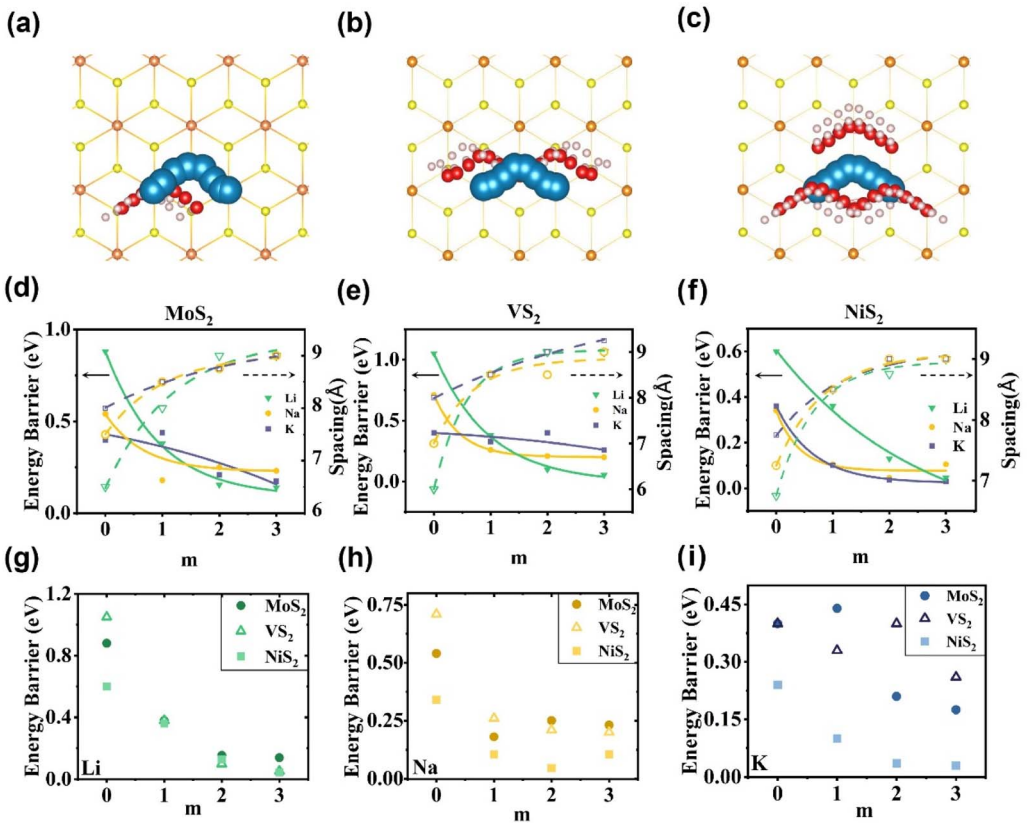

Fig. 4 Hydration-dependent diffusion mechanisms. Schematic diagrams illustrating the proposed diffusion pathways for alkali metal ions coordinated with (a) $m = 1$, (b) $m = 2$, (c) $m = 3$ water molecules ($Y{\cdot}mH_2O$) within the MS_2 interlayer. For (d) MoS_2, (e) VS_2, and (f) NiS_2, the diffusion energy barriers (solid lines) and interlayer spacings (dashed lines) are plotted against the hydration number (m), demonstrating a significant reduction in barrier with increasing hydration. The left and right Y-axes represent energy barrier and spacing, the solid black arrow corresponds to the left axis, whilst the dotted black arrow corresponds to the right axis. The influence of hydration (0–3 H_2O molecules) on the migration barrier of (g) Li, (h) Na, and (i) K ions in MS_2.

molecules expands the distance between the two-dimensional sulfide layers, and there are fewer physical obstacles to the migration of ions between the layers. Conversely, ion migration is typically hindered by interlayer van der Waals forces. The insertion of water molecules weakens these forces and expands the interlayer channel, facilitating the diffusion of alkali metal ions. Fig. 4(g–i) shows a comparison of the diffusion barrier of the same alkali metal ions in different materials. The variation in diffusion barriers across the materials is minimal for Li with 1–3 water molecules but becomes progressively larger for Na and K. This disparity is likely due to the increasing ionic radius, which enhances the ion's sensitivity to the local atomic environment during migration, resulting in a wider distribution of energy barriers. We systematically investigated the origin of hydration-dependent diffusion barrier reduction of alkali metal ions in 1T-MoS_2 interlayers through hydrogen bond network analysis and electronic structure calculations. As shown in Fig. S2, with increasing hydration number, adjacent hydrated Li and Na ions form a continuous interlayer hydrogen-bond network *via* O–H···O hydrogen bonds, which stabilizes the ion hydration shell and provides a low-barrier migration path to reduce the diffusion barrier. The hydrogen bond formation ability follows Li > Na, consistent with the barrier reduction trend, confirming the critical role of the hydrogen-bond network besides interlayer spacing expansion. Differential charge density analysis (Fig. S3) further reveals the intrinsic mechanism: bare Li exhibits strong chemisorption and charge transfer with the MoS_2 substrate, corresponding to a high diffusion barrier; while with increasing hydration, charge redistribution is confined within the hydrated ion complex, and the interfacial interaction shifts to weak van der Waals force, which is the essential reason for the significantly reduced migration barrier of hydrated ions.

Since water addition facilitates alkali metal ion migration in two-dimensional sulfides, the maximum hydration capacity of the interlayer space becomes a critical factor governing overall battery performance. The binding energies for the intercalation with the number of hydrated alkali ions (each with 3 water molecules) into the MS_2 interlayer were calculated. Fig. 5(a–c) shows the relation of binding energy for each intercalated hydrated ion with the total number of intercalated hydrated ions. For Na in MoS_2, the binding energy drops from 4.23 eV to 3.62 eV with the fifth hydrated ion. This decrease indicates that the intercalation of five hydrated ions is excessive and destabilizes

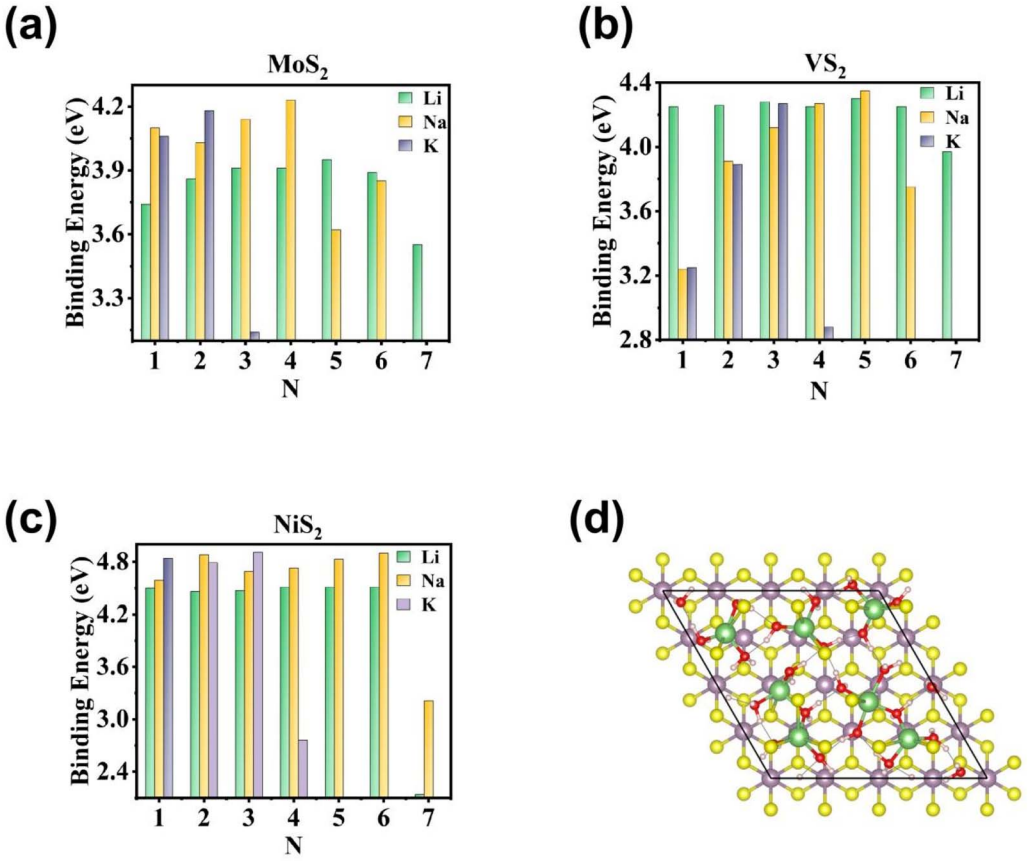

Fig. 5 The average binding energy $\left(\frac{E[(Y\cdot mH_2O)MS_2] - E[MS_2] - E[Y\cdot mH_2O]}{m}\right)$ for each intercalated hydrated ion with the total number of hydrated ions (N) in a 4 × 4 unit cell of (a) MoS_2, (b) VS_2, (c) NiS_2. (d) Schematic diagram of a disordered structure of $(Li\cdot 3H_2O)_7$ in a 4 × 4 unit cell of MoS_2.

the layered structure. When the number of hydrated ions increases to six, the binding energy rebounds to 3.85 eV. This rebound is indicative of excess water molecules self-assembling into a multilayered, hydrogen-bonded network with a distorted geometry. For K, the binding energy is reduced from 4.18 eV to 3.14 eV with the third hydrated ions, where the intercalated structure is compromised. Although the binding energy for Li does not exhibit a clear trend, analysis of the optimized atomic structure reveals a distinct disruption of the interlayer framework upon the intercalation of seven water molecules. Fig. 5(d) shows the disordered interlayer structure of the 4 × 4 MoS_2 unit cell caused by the intercalation of seven hydrated Li ions ($Li\cdot 3H_2O$), which is a result of exceeding the maximum stable accommodation capacity of MoS_2 for hydrated Li ions. This disorder manifests as a marked structural deformation of the hydrated Li ions ($Li\cdot 3H_2O$), which no longer adopt a planar triangular structure; this is induced by the strong steric repulsion caused by the intercalation of excess hydrated ions. This structural disorder further explains the indistinct trend in Li binding energy observed in Fig. 5(a), as the unstable, disordered system leads to anomalous variations in intercalation binding energy. We also analyzed the lengths of the hydrogen bonds formed by water molecules. Table S2 shows that, for all systems, the hydrogen bond lengths decrease as the number of hydrated ions increases. Furthermore, Na exhibits weaker hydrogen-bonding ability than Li, and no stable hydrogen bonds were detected when the number of hydrated ions was high.

As summarized in Fig. 5, the maximum capacity for hydrated (Li, Na, K) ions in a 4 × 4 unit cell of MoS_2 was 6, 4, 2, respectively, while 6, 5, 3 in VS_2 and 6, 6, 3 in NiS_2. This trend highlights the critical role of ionic size in determining the stable hydration structure within the confined interlayer space. The results indicate that 2D-MS_2 materials can accommodate the largest number of hydrated Li ions, followed by Na and then K. This trend is directly determined by ionic radius; the smaller Li ion allows more hydrated complexes to coexist within the interlayer, while the larger K ion is sterically hindered from doing so. Consequently, to enhance performance, Li ion batteries could utilize a highly hydrated electrolyte to accelerate interlayer diffusion. In contrast, K ion batteries require electrolytes with minimal water content to mitigate the limited hydration capacity of K ions. Consequently, the insights from this work open a new avenue for the design of advanced energy-storage materials, where tuning the hydration level of the electrolyte and the host material's interlayer spacing can be leveraged to optimize ionic conductivity.

4 Conclusion

This study revealed the effect of water molecules on the diffusion of alkali metal ions in two-dimensional sulfides. We calculated the diffusion barriers of hydrated Li, Na, and K with 1–3 water molecules in the 2D transition metal sulfides. It was found that the existence of water molecules is conducive to the diffusion of alkali metal ions. In particular, the diffusion barrier decreases as the number of water molecules increases, and when the number of water molecules increases to three, the diffusion barrier can be reduced to close to zero. These findings indicate that two-dimensional sulfide represents a competitive candidate for aqueous battery cathode applications.

Author contributions

Jing Tian contributed to the analysis of the results and to the writing of the manuscript. Xiao Gu conceived the original and supervised the project.

Conflicts of interest

The authors declare that they have no affiliations with or involvement in any organization or entity with any financial interest in the subject matter or materials discussed in this manuscript.

Data availability

Data available within the article.

Supplementary information (SI) is available. See DOI: https://doi.org/10.1039/d6ra00840b.

Acknowledgements

This study was supported financially by the National Natural Science Foundation of China (No. 12274246). All calculations were performed at the Supercomputing Center of Ningbo University and Ningbo Artificial Intelligence Supercomputing Center.

References

1 S. Davoodi, M. Al-Shargabi, D. A. Wood, V. S. Rukavishnikov and K. M. Minaev, Review of technological progress in carbon dioxide capture, storage, and utilization, *Gas Sci. Eng.*, 2023, **117**, 205070.

2 A. Ahmed, T. Ge, J. Peng, W. C. Yan, B. T. Tee and S. You, Assessment of the renewable energy generation towards net-zero energy buildings: A review, *Energy Build.*, 2022, **256**, 111755.

3 J. B. Goodenough and K. S. Park, The Li-ion rechargeable battery: a perspective, *J. Am. Chem. Soc.*, 2013, **135**(4), 1167–1176.

4 M. Armand and J. M. Tarascon, Building better batteries, *Nature*, 2008, **451**(7179), 652–657.

5 B. Dunn, H. Kamath and J. M. Tarascon, Electrical energy storage for the grid: a battery of choices, *Science*, 2011, **334**(6058), 928–935.

6 N. Yabuuchi, K. Kubota, M. Dahbi and S. Komaba, Research development on sodium-ion batteries, *Chem. Rev.*, 2014, **114**(23), 11636–11682.

7 S. W. Kim, D. H. Seo, X. Ma, G. Ceder and K. Kang, Electrode materials for rechargeable sodium-ion batteries: potential alternatives to current lithium-ion batteries, *Adv. Energy Mater.*, 2012, **2**(7), 710–721.

8 M. D. Slater, D. Kim, E. Lee and C. S. Johnson, Sodium-ion batteries, *Adv. Funct. Mater.*, 2013, **23**(8), 947–958.

9 H. Kim, J. C. Kim, M. Bianchini, D. H. Seo, J. Rodriguez-Garcia and G. Ceder, Recent progress and perspective in electrode materials for K-ion batteries, *Adv. Energy Mater.*, 2018, **8**(9), 1702384.

10 S. Chen, M. Zhang, P. Zou, B. Sun and S. Tao, Historical development and novel concepts on electrolytes for aqueous rechargeable batteries, *Energy Environ. Sci.*, 2022, **15**(5), 1805–1839.

11 Z. Liu, Y. Huang, Y. Huang, Q. Yang, X. Li, Z. Huang and C. Zhi, Voltage issue of aqueous rechargeable metal-ion batteries, *Chem. Soc. Rev.*, 2020, **49**(1), 180–232.

12 F. Zheng, M. Kotobuki, S. Song, M. O. Lai and L. Lu, Review on solid electrolytes for all-solid-state lithium-ion batteries, *J. Power Sources*, 2018, **389**, 198–213.

13 C. Cao, Z. B. Li, X. L. Wang, X. B. Zhao and W. Q. Han, Recent advances in inorganic solid electrolytes for lithium batteries, *Front. Energy Res.*, 2014, **2**, 25.

14 M. Galiński, A. Lewandowski and I. Stępniak, Ionic liquids as electrolytes, *Electrochim. Acta*, 2006, **51**(26), 5567–5580.

15 C. Wessells, R. A. Huggins and Y. Cui, Recent results on aqueous electrolyte cells, *J. Power Sources*, 2011, **196**(5), 2884–2888.

16 H. Manjunatha, G. S. Suresh and T. V. Venkatesha, Electrode materials for aqueous rechargeable lithium batteries, *J. Solid State Electrochem.*, 2010, **15**(3), 431–445.

17 W. Tang, Y. Zhu, Y. Hou, L. Liu, Y. Wu, K. P. Loh, H. Zhang and K. Zhu, Aqueous rechargeable lithium batteries as an energy storage system of superfast charging, *Energy Environ. Sci.*, 2013, **6**(7), 2093–2104.

18 J. Xu, X. Cai, S. Cai, Y. Shao, C. Hu, S. Lu and S. Ding, High-energy lithium-ion batteries: recent progress and a promising future in applications, *Energy Environ. Mater.*, 2023, **6**(5), e12450.

19 Y. He, B. Matthews, J. Wang, L. Song, X. Wang and G. Wu, Innovation and challenges in materials design for flexible rechargeable batteries: from 1D to 3D, *J. Mater. Chem. A*, 2018, **6**(3), 735–753.

20 V. Aravindan, P. Sennu, Y. S. Lee and S. Madhavi, Practical Li-ion battery assembly with one-dimensional active materials, *J. Phys. Chem. Lett.*, 2017, **8**(17), 4031–4037.

21 T. T. Mishra, M. Chakraborty, J. Behera and D. Roy, Comprehensive review on bimetallic (Ni and Co)-chalcogenides and phosphides with three-dimensional architecture for hybrid supercapacitor application, *Energy Fuels*, 2024, **38**(11), 9186–9217.

22 E. Pomerantseva and Y. Gogotsi, Two-dimensional heterostructures for energy storage, *Nat. Energy*, 2017, **2**(7), 17089.
23 C. Chowdhury and A. Datta, Exotic physics and chemistry of two-dimensional phosphorus: phosphorene, *J. Phys. Chem. Lett.*, 2017, **8**(13), 2909–2916.
24 R. Rojaee and R. Shahbazian-Yassar, Two-dimensional materials to address the lithium battery challenges, *ACS Nano*, 2020, **14**(3), 2628–2658.
25 P. Wang, H. Sun, Y. Ji, W. Li and X. Wang, Three-dimensional assembly of single-layered MoS_2, *Adv. Mater.*, 2013, **26**(6), 964–969.
26 Y. Li, F. Wu, J. Qian, M. Zhang, Y. Yuan, Y. Bai and C. Wu, Metal chalcogenides with heterostructures for high-performance rechargeable batteries, *Small Sci.*, 2021, **1**(9), 2100012.
27 C. Xie, P. Yang, Y. Huan, F. Cui and Y. Zhang, Roles of salts in the chemical vapor deposition synthesis of two-dimensional transition metal chalcogenides, *Dalton Trans.*, 2020, **49**(30), 10319–10327.
28 X. Chen and R. Fan, Low-temperature hydrothermal synthesis of transition metal dichalcogenides, *Chem. Mater.*, 2001, **13**(3), 802–805.
29 S. L. Brock, I. U. Arachchige and K. K. Kalebaila, Metal chalcogenide gels, xerogels and aerogels, *Comments Inorg. Chem.*, 2006, **27**(5–6), 103–126.
30 P. Chong, Z. Zhou, K. Wang, W. Zhai, Y. Li, J. Wang and M. Wei, The stabilizing of 1T-MoS_2 for all-solid-state lithium-ion batteries, *Batteries*, 2022, **9**(1), 26.
31 X. Lv, W. Guo, J. Song and Y. Fu, Dynamic 1T-2H Mixed-Phase MoS_2 Enables High-Performance Li-Organosulfide Battery, *Small*, 2022, **18**(1), 2105071.
32 P. Kumar, N. C. Verma, N. Goyal, J. Biswas, S. Lodha, C. K. Nandi and V. Balakrishnan, Phase engineering of seamless heterophase homojunctions with co-existing 3R and 2H phases in WS_2 monolayers, *Nanoscale*, 2018, **10**(7), 3320–3330.
33 S. Gao, S. Chen, F. Shi, W. Jiang and J. Chen, Synthesis of 1T-MoS_2 sheets with large space distance between layers for high-rate aqueous Zn-ion batteries cathode, *J. Power Sources*, 2024, **591**, 233866.
34 W. Ding, L. Hu, J. Dai, X. Tang, R. Wei, Z. Sheng, C. Liang, D. Shao, W. Song and Q. Liu, Highly ambient-stable 1T-MoS_2 and 1T-WS_2 by hydrothermal synthesis under high magnetic fields, *ACS Nano*, 2019, **13**(2), 1694–1702.
35 G. Kresse and J. Hafner, Ab initio molecular dynamics for liquid metals, *Phys. Rev. B: Condens. Matter Mater. Phys.*, 1993, **47**(1), 558.
36 G. Kresse and J. Hafner, Ab initio molecular-dynamics simulation of the liquid-metal–amorphous-semiconductor transition in germanium, *Phys. Rev. B: Condens. Matter Mater. Phys.*, 1994, **49**(20), 14251.
37 P. J. Perdew, K. Burke and M. Ernzerhof, Generalized Gradient Approximation Made Simple, *Phys. Rev. Lett.*, 1996, **77**(18), 3865.
38 P. E. Blöchl, Projector augmented-wave method, *Phys. Rev. B: Condens. Matter Mater. Phys.*, 1994, **50**(24), 17953–17979.
39 S. Grimme, J. Antony, S. Ehrlich and H. Krieg, A consistent and accurate ab initio parametrization of density functional dispersion correction (DFT-D) for the 94 elements H-Pu, *J. Chem. Phys.*, 2010, **132**(15), 154104.
40 S. Grimme, Accurate description of van der Waals complexes by density functional theory including empirical corrections, *J. Comput. Chem.*, 2004, **25**(12), 1463–1473.
41 J. Zhang, X. Lu, J. Zhang, H. Li, B. Huang, B. Chen, J. Zhou and S. Jing, Metal-Ions Intercalation Mechanism in Layered Anode From First-Principles Calculation, *Front. Chem.*, 2021, **9**, 677620.
42 J. W. González, E. Flórez and J. D. Correa, MoS_2 2D-polymorphs as Li-/Na-ion batteries: 1T' vs 2H phases, *J. Mol. Liq.*, 2024, **396**, 123904.
43 S. Liao, W. Zhao and X. Gu, Morphology and selectivity of hydrated alkali metal ions as depth of discharge in the 1T-MoS_2 electrode with aqueous electrolytes, *Phys. Chem. Chem. Phys.*, 2024, **26**(14), 11094–11104.